12-2017

Complement 3a Receptor in Dorsal Horn Microglia Mediates Pronociceptive Neuropeptide Signaling

Suzanne Doolen
University of Kentucky, suzanne.doolen@uky.edu

Jennifer Cook
University of Minnesota - Twin Cities

Maureen Riedl
University of Minnesota - Twin Cities

Kelley Kitto
University of Minnesota - Twin Cities

Shinichi Kohsaka
National Institute of Neuroscience, Japan

See next page for additional authors

Authors
Suzanne Doolen, Jennifer Cook, Maureen Riedl, Kelley Kitto, Shinichi Kohsaka, Christopher N. Honda, Carolyn A. Fairbanks, Bradley K. Taylor, and Lucy Vulchanova

Complement 3a Receptor in Dorsal Horn Microglia Mediates Pronociceptive Neuropeptide Signaling

Notes/Citation Information
Published in *GLIA*, v. 65, issue 12, p. 1976-1989.

Digital Object Identifier (DOI)
https://doi.org/10.1002/glia.23208

HHS Public Access

Author manuscript

Glia. Author manuscript; available in PMC 2018 December 01.

Published in final edited form as:

Glia. 2017 December ; 65(12): 1976–1989. doi:10.1002/glia.23208.

Complement 3a receptor in dorsal horn microglia mediates pronociceptive neuropeptide signaling

Suzanne Doolen[1,*], **Jennifer Cook**[2,*], **Maureen Riedl**[3], **Kelley Kitto**[3], **Shinichi Kohsaka**[4], **Christopher N. Honda**[3], **Carolyn A. Fairbanks**[3,5,6], **Bradley K. Taylor**[1,†], and **Lucy Vulchanova**[3,†]

[1]Department of Physiology, University of Kentucky, 800 Rose Street, Lexington, Kentucky 40536-0298

[2]Graduate Program in Neuroscience, University of Minnesota, Minneapolis, Minnesota

[3]Departments of Neuroscience, University of Minnesota, Minneapolis, Minnesota 55455

[4]National Institute of Neuroscience, Tokyo, Japan

[5]Departments of Pharmaceutics, University of Minnesota, Minneapolis, Minnesota 55455

[6]Departments of Pharmacology, University of Minnesota, Minneapolis, Minnesota 55455

Abstract

The complement 3a receptor (C3aR1) participates in microglial signaling under pathological conditions and was recently shown to be activated by the neuropeptide TLQP-21. We previously demonstrated that TLQP-21 elicits hyperalgesia and contributes to nerve injury-induced hypersensitivity through an unknown mechanism in the spinal cord. Here we determined that this mechanism requires C3aR1 and that microglia are the cellular target for TLQP-21. We propose a novel neuroimmune signaling pathway involving TLQP-21-induced activation of microglial C3aR1 that then contributes to spinal neuroplasticity and neuropathic pain. This unique dual-ligand activation of C3aR1 by a neuropeptide (TLQP-21) and an immune mediator (C3a) represents a potential broad-spectrum mechanism throughout the CNS for integration of neuroimmune crosstalk at the molecular level.

Keywords

calcium imaging; neuroimmune; pain

Correspondence: Lucy Vulchanova, 6-145 Jackson Hall, 321 Church St. SE, Minneapolis, MN 55455. vulch001@umn.edu.

*Co-first author

†Co-senior author

ORCID

Suzanne Doolen http://orcid.org/0000-0003-1843-7510

Lucy Vulchanova http://orcid.org/0000-0002-6577-4467

1 INTRODUCTION

The complement 3a receptor (C3aR1) was originally identified as the cognate G-protein coupled receptor for complement component 3a (C3a). C3aR1 was recently shown to also bind the neuropeptide TLQP-21 (Cero et al., 2014; Hannedouche et al., 2013). TLQP-21 is generated from the neurotrophin-inducible protein VGF (nonacronymic), which has been implicated in neuroplasticity associated with learning and memory, depression, and chronic pain (Bartolomucci et al., 2006; Hunsberger et al., 2007; La Croix-Fralish, Austin, Zheng, Levitin, & Mogil, 2011; Lin et al., 2015; Moss et al., 2008; Riedl et al., 2009; Thakker-Varia et al., 2007). TLQP-21 and C3a have a competitive relationship at the same binding site within C3aR1 (Cero et al., 2014; Hannedouche et al., 2013).

Microglial signaling is a crucial factor in the response of the central nervous system (CNS) to injury and disease. In the dorsal horn, microglia mediate neuroinflammation in chronic pain states such as neuropathic pain (Ji, Xu, & Gao, 2014; Taves, Berta, Chen, & Ji, 2013). C3aR1 participates in microglial signaling under pathological conditions including neurodegeneration and virus-induced cognitive impairment (Lian et al., 2016; Vasek et al., 2016). Although the complement system has been implicated in mechanisms of neuropathic pain (Griffin et al., 2007; Liu et al., 1995; Twining et al., 2005), the potential relevance of microglial C3aR1 in dorsal horn has not been addressed. We developed a simple and powerful new application of wide-field Ca^{2+} imaging to monitor C3aR1-mediated microglial activity in spinal cord slices from mice that express eGFP under the control of the Iba1 promoter.

TLQP-21 modulates nociceptive signaling and nerve injury-induced hypersensitivity through both peripheral and spinal mechanisms (Chen et al., 2013; Fairbanks et al., 2014; Rizzi et al., 2008). We previously demonstrated that TLQP-21 elicits hyperalgesia and participates in nerve injury-induced hypersensitivity through an unknown mechanism in the spinal cord (Fairbanks et al., 2014). In the present study, we addressed the hypothesis that microglial C3aR1 is central to this mechanism.

2 MATERIALS AND METHODS

2.1 Animals

All work with animals adhered to the guidelines of the Committee for Research and Ethical Issues of the International Association for the Study of Pain and was approved by the Institutional Animal Care and Use Committee at the University of Minnesota (UofM) and/or University of Kentucky (UK) in accordance with American Veterinary Medical Association guidelines. ICR/CD-1 outbred mice were purchased from Envigo (Indianapolis, USA). C57/Bl6 mice were purchased from Charles-River (Indianapolis, USA). Iba1-eGFP, generated on a C57/Bl6 background, were provided by Dr. Kohsaka, National Institute of Neuroscience, Tokyo, Japan (Hirasawa et al., 2005). Colonies were first established at the UofM, and then breeders were sent to UK. Heterozygous mice were used for all experiments. C3aR1 knock-out mice on a Balb/cJ background and wild-type Balb/cJ were obtained from Jackson Labs (# 005712).

2.2 *In vivo* pharmacological treatments

TLQP-21 (name derived from the four amino acids at the N-terminus of the peptide and the number of amino acids) and TLQP-R21A were obtained from Aapptec (Louisville, KY). The peptides were administered to the intrathecal (i.t.) space in awake male ICR/CD-1 (20–25 g, Envigo) by direct lumbar puncture, as described previously (Fairbanks, 2003; Hylden & Wilcox, 1981). The C3aR1 antagonist SB290157 (Cayman Chemical, Ann Arbor, MI) was dissolved in DMSO and then diluted to a final concentration of 5% DMSO (highest dose) or less (serial dilutions for lower doses) with 0.9% normal saline, pH 7.2. SB290157 was administered (i.t.) 5 min prior to TLQP-21 (i.t.) (Fairbanks et al., 2014) followed by heat hyperalgesia testing (Figure 2a); in nerve-injured mice the antagonist was injected i.t. after measurement of predrug mechanical thresholds (Figure 2c).

2.3 Heat hyperalgesia testing

Heat hyperalgesia was assessed by measuring tail flick latency (TFL) in response to warm water (49°C) tail immersion at baseline (single measurement within 30 min of drug injection) and at selected time points postinjection as indicated in Figure 2. TFL was measured with a stopwatch by an experimenter (KK) blinded to experimental group by another experimenter (CAF). Data are represented as the change in TFL from baseline (experimental TFL – baseline TFL).

2.4 Spared nerve injury (SNI) model

The spared nerve injury model is a well-established model that produces substantial and prolonged changes in mechanical sensitivity and cold responsiveness that closely mimic the cutaneous hypersensitivity associated with clinical neuropathic pain (Decosterd & Woolf, 2000). SNI or sham surgery were performed under isoflurane anesthesia as described (Bourquin et al., 2006). For RNA analysis and immunohistochemistry, SNI was performed at 35 days of age. For calcium imaging, we performed SNI at a younger age (25 days). SNI performed at this age yields both tactile hypersensitivity and spinal cord slices that are compatible with Fura-2 AM loading and calcium imaging (Doolen, Blake, Smith, & Taylor, 2012). For calcium imaging and qPCR, mice were sacrificed at 2 weeks post-SNI, and fresh tissue was collected for either slice preparation or RNA extraction. To assess the time course of C3aR1 expression, mice were sacrificed by transcardial perfusion at 3, 14, and 28 days post-SNI.

2.5 Mechanical threshold testing

Mice were acclimated at least 30 min in the testing environment within a plastic box on a raised metal mesh platform. Mechanical thresholds were tested using either an electronic von Frey aesthesiometer (UofM) (IITC Life Sciences, Woodland Hills, CA, USA) or von Frey filaments (UK). For electronic von Frey measurements, the probe was gently applied to the plantar surface of each hind paw until a brisk withdrawal response terminated application of pressure; this pressure threshold was recorded. For manual von Frey testing, a logarithmically increasing set of 8 von Frey filaments (Stoelting, Illinois), labeled from 0.007 to 6.0 g were utilized. These were applied perpendicular to the ventral-medial hindpaw surface with sufficient force to cause a slight bending of the filament. A rapid

withdrawal of the paw away from the stimulus fiber within 4 s was deemed as a positive response. Using an up-down statistical method (Chaplan, Bach, Pogrel, Chung, & Yaksh, 1994), the 50% withdrawal threshold was calculated for each mouse and then averaged within the experimental groups. Mechanical hypersensitivity was confirmed in all SNI mice used in this study.

2.6 Spinal cord slice preparation and fluorometric Ca^{2+} measurements

Mice were anesthetized with 5% isoflurane and quickly perfused transcardially with 10 mL of icecold sucrose-containing artificial cerebrospinal fluid (aCSF) (sucrose aCSF) that contained (in mM): NaCl 95, KCl 1.8, KH_2PO_4 1.2, $CaCl_2$ 0.5, $MgSO_4$ 7, $NaHCO_3$ 26, glucose 15, sucrose 50, kynurenic acid 1, oxygenated with 95% O_2/5% CO_2; pH 7.4. The lumbar spinal cord was rapidly isolated by laminectomy from the cervical enlargement to the cauda equina, placed in oxygenated icecold sucrose-aCSF, cleaned of dura mater and ventral roots, and super-glued vertically to a block of 4% agar (Fisher Scientific, Pittsburgh, PA) on the stage of a Campden 5000 mz vibratome (Lafayette, IN). Transverse spinal cord slices (450 μm) were incubated for 60 min at room temperature with Fura-2 AM (10 μM) and pluronic acid (0.1%) in normal aCSF containing (in mM): NaCl 127, KCl 1.8, KH_2PO_4 1.2, $CaCl_2$ 2.4, $MgSO_4$ 1.3, $NaHCO_3$ 26, glucose 15, and oxygenated with 95% O_2/5% CO_2. This was followed by a 20 min de-esterification period in normal aCSF. Within 8 h, slices were perfused at 1–2 mL/min with normal aCSF in an RC-25 recording chamber (Warner Instruments, Hamden, CT) mounted on a Nikon FN-1 upright microscope fitted with a 79000 ET FURA2 Hybrid filter set (Nikon Instruments, Melville, NY) and a PhotometricsCoolSNAP HQ2 camera (Tucson, AZ). Paired images at 340 and 380 nm were collected at 1–1.5 s/frame. Relative changes in the number and peak amplitude of Ca^{2+} transients in Fura-2 labeled cells were evaluated using Nikon Elements software. Profiles that displayed changes in peak Ca^{2+} amplitude 3% above baseline in response to TLQP-21 or glutamate exposure were considered to have a positive response. The 3% above baseline cutoff was approximately twofold greater than noise, defined as the difference between the maximum and minimum baseline values during the 30-s period preceding drug application. Typically, one slice was used per treatment per mouse, and all values comprise the average value of all profiles analyzed within that mouse. In R21A mutant peptide studies, we exposed single slices to R21A followed by 1 μM TLQP-21 in order to compare Ca^{2+} transients produced by the two peptides.

2.7 Real-time quantitative PCR (qPCR)

Two weeks post-SNI, spinal cords were removed via hydraulic extrusion. The lumbar enlargements were dissected and split along the mid-line into ipsilateral and contralateral halves relative to the peripheral injury. After homogenization, RNA was extracted with the Qiagen RNA Easy Lipid Mini Kit (Qiagen) and purified with the TURBO DNA free kit (Thermo Scientific). cDNA was generated with the Roche Transcriptor First Strand cDNA synthesis kit (Roche), and quantitative real-time PCR was performed on a LightCycler 480 machine using primers for C3aR1 and GAPDH and the Roche LightCycler 480 SYBR Green Master Mix (Roche). Primer sequences were: C3aR1: 5′-ACAAGTGAGACC AAGAATGACC-3′ and 5′-GATTCCATCTCAGTGTGCTTG-3′. GAPDH: 5′-GTGGAGTCATACTGGAACATGTAG-3′ and 5′-AATGGTGAAGGTC GGTGTG-3′.

ΔΔCT values were calculated for each condition using sham contralateral as the control group. Fold changes ($2^{\Delta\Delta CT}$) for each group were compared with a one-way ANOVA, followed by Tukey's *post hoc* test.

2.8 Primary microglial cultures

Cortical cells were collected from postnatal day 1–3 mouse pups of both sexes (CD-1, Charles River; Balb c/J wild-type or C3aR1 knockout, Jackson Laboratory) and plated under conditions that promote survival of glial cells but not neurons (Skaper, Argentini, & Barbierato, 2012). Mixed glial cultures were maintained in EMEM +10% fetal bovine serum (FBS) +1% L-glutamine +1% Penstrep (EMEM, 500 mL, Gibco; FBS, Gibco, 26140–079; L-glutamine, 200 mM, Thermo Fisher; Penstrep, Gibco) at 37°C. After approximately 2 weeks, the flasks were shaken at 200 rpm for 1.5 h to detach microglia. Each flask contained cells from approximately two pups and yielded approximately four coverslips. Cells were plated on 25 mm coverslips coated with poly-D-lysine (Sigma) at a density of 45,000 cells per coverslip. Cells were kept at 37°C for 72 h prior to calcium imaging. The primary cultures consisted of approximately 98% microglia.

2.9 Primary microglia Ca^{2+} imaging

Cultured primary microglia were used 72 h after plating. Coverslips were incubated with the ratiometric intracellular calcium indicator Fura-2 AM (Invitrogen) at a final concentration of 1.5 μM in HEPES buffer containing 1% bovine serum albumin for 20 min prior to calcium imaging. Coverslips were then transferred to a recording chamber and perfused at a rate of 1.8 mL/min with HEPES–Hank's buffer (25 mM HEPES, 135 mM NaCl, 2.5 mM $CaCl_2$, 3.5 mM KCl, 1 mM $MgCl_2$, and 3.3 mM glucose, pH 7.4 and 335–340 mOsm adjusted with sucrose). A single field of view containing approximately 8 cells was imaged in each coverslip. Experimenters chose fields of view based on microglia cell morphology, such as resting elongated cells and rounded cells. Cells were exposed to 100 μM ATP at 60 s and 10 μM TLQP-21 at 660 s during the recording session. Excitation wavelengths of 340 and 380 were used to measure bound and unbound calcium, respectively, in order to examine calcium flux. Excitation wavelengths and shutter speed were controlled by a DeltaRam X controller and LPS-220B lamp (PTI). ImageMaster 5.0 software (PTI) was used to collect and analyze all images. Ratios of 340/380 were calculated and differences between the amplitude ratios at baseline and at peak after stimulation were measured in each cell within the field of view. Cells were considered responsive to ATP or TLQP-21 if the peak amplitude was twofold greater than noise, defined as the difference between the maximum and minimum baseline values during the 10-s period preceding drug application. Three to five coverslips were tested from three CD-1 WT, three C3aR1 WT, and three C3aR1 KO cultures. Cells were grouped into responders or nonresponders in a contingency table for each treatment and were compared using Fisher's exact test.

2.10 Immunohistochemistry

Mice were deeply anesthetized with isoflurane and perfused via the heart with calcium-free Tyrode's solution (in mM: 116 NaCl, 5.4 KCl, $1.6\,MgCl_2 6H_2O, 0.4\,MgSO_4 7H_2O$, 1.4 NaH_2PO_4, 5.6 glucose, and 26 Na_2HCO_3) followed by fixative (4% paraformaldehyde and

0.2% picric acid in 0.1M phosphate buffer, pH 6.9). Tissues were dissected, incubated in 10% sucrose overnight at 4°C, and then cryostat-sectioned (14 μm) and thaw-mounted on to gelatin-coated slides. Sections were preabsorbed in blocking buffer (PBS containing 0.3% Triton-X 100, 1% BSA, 1% normal donkey serum) for 30 min, incubated in primary antibodies overnight at 4°C, rinsed with PBS 3 × 10 min, incubated in secondary antisera (1:300, Jackson ImmunoResearch, West Grove, CA) for 1 h at room temperature, washed with PBS, and coverslipped using PBS/glycerol containing 0.1% *p*-phenylenediamine (Sigma). Primary antibodies included: rat anti-C3aR1 (1:100, Hycult Biotech), rabbit anti-Iba1 (1:1000; Wako Chemicals), goat anticollagen IV (1:2500, SouthernBiotech), mouse anti-GFAP (1:1000, Sigma), mouse anti-MAP2 (1:5000; Millipore), and rabbit anti-NeuN (1:1000, Cell Signaling). Images were collected with an Olympus FluoView1000 confocal imaging system. Adjustments of contrast and brightness were performed in Adobe Photoshop CS5; images from wild type and knockout mice were adjusted identically. For quantification of colocalization of Iba1 and GFP labeling in Iba1-eGFP mice, images of dorsal horn were collected as z-stacks (6 optical sections, 1 μm apart) and projected in Image J. Three nonadjacent sections of lumbar spinal cord were imaged for each subject ($n = 3$). The projected images were thresholded above the level of background staining intensity, using the same threshold value for all Iba1 and GFP images, respectively. Stacks of corresponding Iba1 and GFP images were created in Image J. Cellular profiles, identified based on the presence of a soma-like structure with associated processes, were outlined and assessed for presence of Iba1 and GFP labeling. Labeled profiles were counted, and the average number of double-labeled and single-labeled profiles per section was calculated for each subject. For quantitative image analysis of C3aR1-ir, single optical sections of C3aR1/Iba1/MAP2 triple-labeling were collected using constant image acquisition settings. Iba1 staining was used for unbiased selection of the focal plane. Analysis was performed in Image J. MAP2 labeling was used for reproducible outlining of a region of dorsal horn that included laminae I–III. To measure the area of C3aR1 labeling, the images were thresholded by a blinded experimenter. Analysis by three different blinded experimenters yielded reproducible results. C3aR1 labeling was expressed as % thresholded area. Data from three nonadjacent L3/L4 sections were averaged from each spinal cord.

2.11 Statistical analysis

Data are expressed as the mean ± SEM, with $p < .05$ as significant. *p* values were determined using *t*-tests for two-group analysis, and 1- or 2-way ANOVA with repeated measures followed by pairwise comparisons using GraphPad Prism software (version 6; GraphPad Software, San Diego, CA). Proportions of profiles/cells were compared using Fisher's exact test.

3 RESULTS

3.1 C3aR1 is expressed in spinal microglia

Although C3aR1 mRNA transcripts have been localized to neurons, astrocytes, and microglia in spinal cord (Davoust, Jones, Stahel, Ames, & Barnum, 1999), much less is known about the spinal distribution of C3aR1 protein. To fill this gap, we characterized a C3aR1 antibody with immunohistochemistry of spinal cord slices. Figure 1 demonstrates

C3aR1 immunoreactivity (–ir) on fine, short processes and a few cellular profiles throughout the spinal cord, including in the dorsal and ventral horn as well as in the white matter. C3aR1-ir was absent in C3aR1 knockout mice, demonstrating antibody specificity (Figure 1a,b). Double labeling for C3aR1 and Iba1, a marker of macrophages and microglia, indicated that C3aR1-ir was almost exclusively associated with microglia (Figure 1c–h, arrowheads). Intense C3aR1 labeling was also present in Iba1-positive meningeal/ subarachnoid monocytes located within the pia mater or in close apposition to subarachnoid blood vessels, as indicated by their proximity to collagen IV-ir (Urabe et al., 2002) (Figure 1c–h, arrows; Figure 1i).

3.2 C3aR1 mediates TLQP-21-induced heat hyperalgesia and contributes to nerve injury-induced hyperalgesia

Intrathecal administration of TLQP-21 induces a transient, prostaglandin-dependent heat hyperalgesia in the warm water tail immersion assay (Fairbanks et al., 2014). To determine if this pronociceptive effect is mediated by C3aR1, the C3aR1 antagonist SB290157 was injected before TLQP-21. Intrathecal SB290157 had no behavioral effect when injected alone, but dose-dependently (0.1–1.0 nmol) inhibited the hyperalgesia induced by TLQP-21 (Figure 2a). To confirm that TLQP-21 signals through C3aR1, we injected an inactive analog of TLQP-21. Substitution of the C-terminal arginine of TLQP-21 with ala-nine yields an analog (R21A) that is unable to activate C3aR1 (Cero et al., 2014). Compared to the robust effect of TLQP-21, R21A produced only a weak heat hyperalgesia (Figure 2b; at 60 min, R21A: −0. 47 ± 0.54, TLQP-21: −2.64 ± 0.2; $p < .001$, two-way repeated measures ANOVA and Bonferroni *post hoc* test).

We previously used an immunoneutralization approach to demonstrate that TLQP-21 is necessary for nerve injury-induced hypersensitivity (Fairbanks et al., 2014). To determine whether C3aR1 signaling is necessary as well, we evaluated the effect of SB290157 in the SNI model of neuropathic pain. SB290157 (1 nmol, i.t.) reversed mechanical hypersensitivity as compared to vehicle (Figure 2c; $p < .01$ at 30 min postdrug, $p < .05$ at 2 h postdrug, two-way repeated measures ANOVA and Bonferroni's *post hoc* test).

3.3 Peripheral nerve injury potentiates spinal TLQP-21-evoked, C3aR1-mediated, Ca^{2+} responses

Using live-cell wide-field Fura-2 ratiometric analysis in adult mouse spinal cord slices (Doolen et al., 2012), we previously reported glutamate-evoked Ca^{2+} signaling in lamina II from lumbar L3/L4 segments. To delineate the cellular mechanisms underlying the spinal effects of TLQP-21 and its contribution to neuropathic pain, we superfused TLQP-21 and then quantified both the number and peak amplitude of evoked Ca^{2+} transients. TLQP-21 evoked a small number of Ca^{2+} transients in slices from sham controls (Figure 3); this was dramatically increased in slices from mice that underwent SNI (Figure 3a; number of cells: 1.0 ± 0.57 sham vs. 10.75 ± 2.3 SNI, $p = .017$, $n = 3–4$ mice/ group). As illustrated in Figure 3b, the TLQP-21 response in SNI mice was concentration-dependent (Figure 3b; EC_{50} = 140.8 nM). SNI increased not only the number of TLQP-21-evoked Ca^{2+} transients, but also their peak amplitude (Figure 3c, 0.026 ± 0.013 sham vs. 0.069 ± 0.006 SNI, $p = .025$, $n = 3–4$ mice/group). These data indicate that nerve injury potentiates TLQP-21 signaling.

To determine whether C3aR1 mediates the cellular effects of TLQP-21 in dorsal horn, we asked whether the C3aR1 antagonist SB290157 would block TLQP-21-induced Ca^{2+} responses. We tested this hypothesis in neuropathic mice to avoid a floor effect associated with the small number of Ca^{2+} transients in uninjured mice. SB290157 (1 μM) reduced both the number of profiles (10.75 ± 2.3 vehicle vs. 2.5 ± 0.64 SB290157; $p = 0.014$, $n = 4$ mice/group) and peak amplitude (0.069 ± 0.006 vehicle vs. 0.018 ± 0.01 SB290157, $p = .006$, $n =$ 3–4 mice/group) of Ca^{2+} responses to 1 μM TLQP-21 (Figure 4a,b). As illustrated with representative Ca^{2+} traces shown in Figure 4c, R21A produced a smaller number of Ca^{2+} transients as compared to TLQP-21 (Figure 4d, 1.4 ± 0.50 with R21A vs. 8.2 ± 1.1 with TLQP-21, $p = .0004$, $n = 5$ mice/group). These data indicate that C3aR1 mediates TLQP-21 signaling in dorsal horn.

3.4 Peripheral nerve injury increases the spinal expression of C3aR1

Next we tested the hypothesis that SNI increases the expression of C3aR1 in dorsal horn. As illustrated in Figure 5a, 14 days after SNI we observed an approximately twofold increase in C3aR1 mRNA in the ipsilateral spinal cord (2.22 ± 0.2) as compared to the contralateral side of SNI mice (1.33 ± 0.25) or the ipsilateral (1.31 ± 0.21) or contralateral (1.07 ± 0.13) spinal cord of sham mice ($p < .001$, $n = 14$–16 mice/ group; one-way ANOVA followed by Tukey's multiple comparisons test). To determine the time course of the increase in spinal C3aR1 expression, we measured the area of C3aR1 labeling in dorsal horn at 3, 14, and 28 days after SNI or sham surgery (Figure 5b). The maximum increase in C3aR1-ir, relative to sham, was observed 3 days after nerve injury. Although the labeling progressively decreased at 14 and 28 days post-SNI, C3aR1 expression remained elevated in the medial portion of dorsal horn as compared to control (Figure 5c–h).

3.5 TLQP-21-evoked Ca^{2+} signaling predominantly occurs in microglia: immunohistochemistry

Having established that C3aR1 is predominantly expressed in microglia and that TLQP-21-evoked behavioral and spinal Ca^{2+} responses are C3aR1-dependent, we next used double-label immunohistochemistry and Ca^{2+} imaging to ask whether activation of the TLQP-21/C3aR1 axis elicits signaling in neurons, astrocytes, and/or microglial cell types.

We found that C3aR1-ir was extensively co-localized with Iba1-ir at all time points examined (14 days post-SNI shown in Figure 6a). In contrast, C3aR1-ir did not co-localize with either the astrocyte marker GFAP or the neuronal marker NeuN (Figure 6b,c). These data indicate that the expression of C3aR1 is limited to microglia, with no evidence of expression in spinal astrocytes or neurons, at least in the setting of nerve injury.

3.6. TLQP-21-evoked Ca^{2+} signaling predominantly occurs in microglia: imaging in spinal cord slices

We extensively analyzed TLQP-21-induced Ca^{2+} transients in spinal cord slices to determine their cellular origin. We first determined whether they occur in astrocytes. As illustrated in Figure 7a–c, real-time double-labeling of Fura-2 with the astrocyte marker SR-101 failed to reveal any overlap, indicating that none of the Fura-2 profiles (0 of 161) were astrocytes.

We next tested if TLQP-21 activates Ca^{2+} responses in neurons. To do this, we directly compared the population of profiles responding to TLQP-21 with the population of profiles that exhibit a high (>10% above baseline) response to glutamate - a population that fires action potentials and are thus categorized as neurons (Doolen et al., 2012). We superfused slices with TLQP-21 (1 μM, 90 s), and then with glutamate (1 mM, 10 s), and analyzed 161 profiles (collected from slices from 7 mice). Profiles were classified as TLQP-21 "responders" if they exhibited increases in Ca^{2+} greater than 3% of baseline (noise accounts for roughly 3% change in baseline). The representative traces shown in Figure 7d–f illustrate Ca^{2+} signaling in individual profiles that did not respond to TLQP-21 but had a high glutamate response (D), or responded to TLQP-21 and had a low (E) or no response (F) to glutamate. As summarized in Table 1, 76 of 161 profiles (47%) responded to TLQP-21 (1 μM) or both TLQP-21 and glutamate, while 85 of 161 profiles (53%) were TLQP-21 nonresponsive. Of the 76 cells that were TLQP-21 responders, glutamate produced no (35 cells) or low (35 cells) Ca^{2+} response. Glutamate produced a high Ca^{2+} response in only 6 of the TLQP-21 responders. In contrast, of the 85 cells that were not TLQP-21 responders, glutamate produced a high Ca^{2+} response in the majority (51) of cells, and a low Ca^{2+} response in the other 34 cells. When we quantified the peak magnitude of Ca^{2+} signal, the response to 1 mM glutamate was significantly lower in the TLQP-21 responsive population as compared to the TLQP-21 nonresponsive population (ratio = 0.032 ± 0.003 vs. 0.098 ± 0.006, respectively; $p < .001$). These data illustrate that TLQP-21 responsive cells typically do not exhibit a high response to glutamate that is characteristic of neurons. These findings suggest that the majority of TLQP-21-responsive profiles belong to a cell population that is largely distinct from the predominantly neuronal population.

Having largely ruled out a contribution of astrocytes or neurons, we next tested the hypothesis that TLQP-21-evoked Ca^{2+} transients occur in microglia. The selectivity of available microglial inhibitors has been widely questioned (Liu, Zhang, Zhu, Luo, & Liu, 2015; Moller et al., 2016; Peng, Ma, Lv, Hu, & Liu, 2016); therefore, we employed mice that express eGFP under the control of the Iba1 promoter (Iba1-eGFP mice). We first characterized these mice with double-label immunohistochemistry of eGFP and Iba1-ir in dorsal horn sections (3 sections/mouse from 3 mice). We found that 95.4% (1107/1160) of Iba1-positive cells were eGFP-positive; conversely, 99.8% (1107/1109) of eGFP-positive cells were Iba1-positive (Figure 7g–j). These data indicate high fidelity in the eGFP labeling of microglia in the dorsal horn of Iba1-eGFP mice. Therefore, we proceeded to characterize Ca^{2+} responses in Iba1-eGFP mice. Figure 7k–m illustrates Fura-2 loading into both eGFP-positive and -negative profiles from these mice; of 29 eGFP-positive cells, we observed that Fura-2 loaded into 23 of them. Figure 7n–o illustrate typical Ca^{2+} transients observed in eGFP-positive and -negative profiles. TLQP-21 evoked Ca^{2+} responses in virtually all eGFP-positive cells that took up Fura-2 (22/23; 95%), and the majority of TLQP-21 responsive profiles were eGFP-positive (22/28; 79%). In contrast, Table 2 illustrates that responses to glutamate in eGFP-positive cells were predominantly low (17/23; 74%) or absent (3/23; 13%), and were very rarely high (2/23; 9%). Similar to wild type mice, the peak magnitude of Ca^{2+} signals in response to 1 mM glutamate was significantly smaller in TLQP-21 responsive profiles compared to TLQP-21 nonresponsive profiles (ratio = 0.035 ± 0.003 vs. 0.085 ± 0.004, $p < .001$, $n = 114$ profiles from 3 mice). Together, these findings indicate that

the majority of TLQP-21 responsive profiles are Iba1-eGFP positive microglia. Our observation of glutamate-evoked Ca^{2+} responses in microglia is consistent with previous studies indicating the presence of microglial glutamate receptors (Beppu et al., 2013; Hagino et al., 2004; Murugan, Sivakumar, Lu, Ling, & Kaur, 2011).

In contrast to the eGFP-positive population, the eGFP-negative population (91 of 114 profiles; 80%) was largely unresponsive to TLQP-21 (85/91; 93%) and exhibited high (53/85) or low (32/85) Ca^{2+} responses to 1 mM glutamate. Notably, the proportions of high and low glutamate responders were significantly different in the GFP positive and negative populations (GFP positive: 9% high, 74% low; GFP-negative: 59% high, 39% low; $p < .0001$, Fisher's exact test). These data suggest that the eGFP-negative population overlaps with a population of glutamate responsive cells that we consider to be neurons (Doolen et al., 2012). They do not, however, indicate that microglial cells are devoid of glutamate-evoked Ca^{2+} responses, because a considerable number of both eGFP-positive and negative cells produced low Ca^{2+} signals in response to glutamate (17 of 22 eGFP-positive; 36 of 91 eGFP-negative cells).

3.7 TLQP-21-evoked Ca^{2+} signaling predominantly occurs in microglia: imaging in microglial cultures

As spinal cord slices contain a complex cellular environment, it is possible that the microglial Ca^{2+} responses to TLQP-21 are secondary to activation of another cell type. To determine whether TLQP-21 is able to directly activate microglia, we next evaluated Ca^{2+} signaling in cortical microglial cultures prepared from neonatal CD-1 mice (P1–3). To restrict our analysis of TLQP-21-evoked responses to viable microglia, we used ATP as a reliable stimulus for microglial Ca^{2+} signaling (Wang, Kim, van Breemen, & McLarnon, 2000). Cells were considered responsive to ATP or TLQP-21 if the peak amplitude was twofold greater than noise. We found that all TLQP-21-responsive cells were ATP-responsive (representative trace shown in Figure 8a). As illustrated by the scatterplots of peak response amplitudes, of 97 cells found to be ATP-responsive, 37 also responded to TLQP-21, while 60 did not (Figure 8b). To determine if these responses were mediated by C3aR1 activation, we tested the effects of the R21A analog. In these experiments, of 78 cells found to be ATP-responsive, only 5 responded to R21A, while 73 did not. Statistical analysis indicated that a significantly lower proportion of cells responded to R21A (6%) compared to TLQP-21 (38%) ($p < .0001$, Fisher's exact test).

We next compared TLQP-21 responses in microglial cultures taken from either C3aR1 knock-out (KO) mice or their Balb/cJ wild-type (WT) controls. Figure 8c and d show scatterplots of peak response amplitudes for ATP and TLQP-21 for responders and nonresponders in WT and KO microglial cultures. Similar proportions of WT (90%) and KO (87%) cells responded to ATP. In contrast, the proportions of TLQP-21 responsive cells in WT (65%) and KO (5%) cultures differed significantly ($p < .0001$, Fisher's exact test). Taken together, these experiments demonstrate that TLQP-21 directly activates C3aR1-dependent Ca^{2+} signaling in microglia.

4 DISCUSSION

C3aR1 has emerged as a neuro-glial mediator that contributes critically to pathological processes in the CNS by regulating neuroinflammation as well as neuronal structure and function (Lian et al., 2015; Vasek et al., 2016). We previously demonstrated that the newly identified ligand of C3aR1, TLQP-21, elicits hyperalgesia and participates in the development and maintenance of nerve injury-induced hypersensitivity (Fairbanks et al., 2014). Here we examined the interaction of TLQP-21 and C3aR1, and provide the first evidence that microglial C3aR1 mediates the effects of TLQP-21 within the central nervous system.

4.1 TLQP-21 activates spinal C3aR1

We show that TLQP-21 signaling in spinal cord is C3aR1-dependent. The C3aR1 antagonist SB290157 blocked both the behavioral (heat hyperalgesia) and cellular (Ca^{2+} signaling) actions of TLQP-21. Notably, these actions were also abolished by a single amino acid substitution in the C-terminus of TLQP-21 (R21A), which eliminates its ability to activate C3aR1 (Cero et al., 2014). Our findings provide *in vivo* confirmation of recent molecular and structural studies indicating that TLQP-21 directly activates C3aR1 (Cero et al., 2014; Hannedouche et al., 2013).

4.2 High fidelity Ca^{2+} imaging in *ex vivo* microglia

Until recently, microglial Ca^{2+} signaling had only been characterized in cultured cells (Farber & Kettenmann, 2006). Here we took advantage of eGFP expression under the control of the Iba1 promoter to perform real-time, wide-field Ca^{2+} imaging of microglial activity with high fidelity in a spinal cord slice preparation for the first time. We found that Fura-2 AM was taken up by 79% of Iba1-eGFP positive cells, accounting for a majority of microglia in the dorsal horn. This represents a powerful and novel approach to directly monitor microglia in an environment where they retain the ability to interact with other cell types, including neurons and astrocytes (Brawek & Garaschuk, 2013; Nimmerjahn, Kirchhoff, & Helmchen, 2005; Tsuda & Inoue, 2016).

4.3 TLQP-21 directly targets C3aR1 to activate spinal microglia rather than neurons

We provide functional and anatomical evidence that microglia in the dorsal horn are the predominant cellular target for the spinal effects of TLQP-21. First, our experiments in Iba1-eGFP mice clearly demonstrate that TLQP-21 elicits Ca^{2+} signaling in microglia. Over 95% of Fura-2 loaded/eGFP-positive profiles responded to TLQP-21, suggesting that Ca^{2+} response to TLQP-21 is predictive of microglial identity. We propose that TLQP-21 can be used in future studies to selectively activate microglia in the dorsal horn. Second, we demonstrate extensive C3aR1 co-localization with Iba1-ir microglia in the dorsal horn. Our co-localization analysis of C3aR1, GFAP, and NeuN labeling did not yield evidence for C3aR1 expression in astrocytes or neurons; however, we cannot rule out a secondary contribution of activation in neurons and/or astrocytes as 17.8% (5/28) of TLQP-21-responsive profiles were eGFP-negative and responded to glutamate. Third, the absence of TLQP-21-elicited Ca^{2+} transients in C3aR1 KO mice and in WT cultures exposed to R21A reinforces the evidence that TLQP-21 signaling is C3aR1-mediated.

4.4 C3aR1 in nerve injury-induced spinal neuroplasticity

Using immunoneutralization, we previously demonstrated that endogenous spinal TLQP-21 contributes to the development and maintenance of nerve injury-induced hypersensitivity (Fairbanks et al., 2014). The present results identify microglial C3aR1 as the pronociceptive target for TLQP-21. Since the TLQP-21 precursor VGF is upregulated in sensory neurons within 24 h of nerve injury (Riedl et al., 2009), spinal TLQP-21 released from injured sensory neurons is positioned to function as an endogenous danger signal that contributes to spinal neuroinflammation after nerve injury through activation of C3aR1.

Little is known about the spinal availability of the originally characterized C3aR1 ligand C3a. Although expression of C3, the precursor of C3a, emerges in spinal microglia three days after peripheral nerve injury (Gattlen et al., 2016; Griffin et al., 2007; Liu et al., 1995; Twining et al., 2005), the generation of C3a or its contribution to hypersensitivity remains to be established.

We found that SNI increased both microglial C3aR1 expression and TLQP-21-evoked C3aR1-dependent Ca^{2+} signaling in the dorsal horn of the spinal cord. Moreover, pharmacological inhibition of C3aR1 attenuated the behavioral hypersensitivity associated with SNI. These results provide the first evidence that microglial C3aR1 contributes to neuropathic pain.

C3aR1 activation of monocytes induces release of ATP and cytokines (Asgari et al., 2013). Spinal microglia also have the capacity to release ATP (Liu, Kalous, Werry, & Bennett, 2006), and microglial purinergic receptors are heavily implicated in neuropathic pain mechanisms (Beggs, Trang, & Salter, 2012). This leads us to speculate that the potential downstream consequences of C3aR1 signaling following nerve injury include microglial release of ATP and cytokines, including mediators of spinal neuroplasticity such as IL-1β (Clark et al., 2015; Gruber-Schoffnegger et al., 2013).

4.5 C3aR1 is expressed in meningeal/subarachnoid monocytes

The present study makes the intriguing and novel observation that C3aR1 is expressed in meningeal/subarachnoid monocytes. It is well documented that monocytes can be found in mouse meninges and human cerebrospinal fluid, and that their number increases in pathological states such as multiple sclerosis (Chinnery, Ruitenberg, & McMenamin, 2010; Polfliet et al., 2001; Waschbisch et al., 2016). Thus, we suggest that C3aR1 is well-positioned to respond to complement pathway activation within the cerebrospinal fluid (e.g., in response to pathogens). Importantly, VGF fragments have been detected in multiple proteomic studies of human CSF (Bartolomucci et al., 2011). Therefore, we speculate that TLQP-21 acts at C3aR1 on monocytes in the CSF to promote neuroinflammation. Furthermore, since activated monocytes release prostaglandins that may diffuse within the spinal cord (Ulmann, Hirbec, & Rassendren, 2010), C3aR1 receptors on CSF monocytes may provide insight into the mechanisms underlying the prostaglandin-mediated thermal hyperalgesia observed following intrathecal injection of TLQP-21 (Fairbanks et al., 2014).

In summary, we show that the spinal mechanisms of pronociceptive actions of TLQP-21 involve direct activation of C3aR1 on microglia. This study provides the first evidence that

microglial C3aR1 contributes to maladaptive changes after neuropathic injury, raising the possibility that C3aR1 may be a novel therapeutic target for the control of chronic pain. Our results are also the first to describe a receptor within the CNS that is activated by both a neuropeptide (TLQP-21) and an immune mediator (C3a). The identification of C3aR1 as the spinal target of TLQP-21 suggests a novel interplay of neuronal and immune signaling mediators in CNS diseases.

Acknowledgments

We thank Galina Kalyuzhnaya for technical assistance. This work was supported by R01 NS088518, K01DA031961 (SD), R01DA37621 (BKT), T32DA007234 (JC), T32GM008471 (JC), F31 NS095421 (JC).

References

Asgari E, Le Friec G, Yamamoto H, Perucha E, Sacks SS, Kohl J, … Kemper C. C3a modulates IL-1beta secretion in human monocytes by regulating ATP efflux and subsequent NLRP3 inflammasome activation. Blood. 2013; 122:3473–3481. https://doi.org/10.1182/blood-2013-05-502229. [PubMed: 23878142]

Bartolomucci A, La Corte G, Possenti R, Locatelli V, Rigamonti AE, Torsello A, … Moles A. TLQP-21, a VGF-derived peptide, increases energy expenditure and prevents the early phase of diet-induced obesity. Proceedings of National Academic Sciences USA. 2006; 103:14584–14589. https://doi.org/10.1073/pnas.0606102103.

Bartolomucci A, Possenti R, Mahata SK, Fischer-Colbrie R, Loh YP, Salton SR. The extended granin family: Structure, function, and biomedical implications. Endocrine Reviews. 2011; 32:755–797. https://doi.org/10.1210/er.2010-0027. [PubMed: 21862681]

Beggs S, Trang T, Salter MW. P2X4R+ microglia drive neuropathic pain. Nature Neuroscience. 2012; 15:1068–1073. https://doi.org/10.1038/nn.3155. [PubMed: 22837036]

Beppu K, Kosai Y, Kido MA, Akimoto N, Mori Y, Kojima Y, … Noda M. Expression, subunit composition, and function of AMPA-type glutamate receptors are changed in activated microglia; possible contribution of GluA2 (GluR-B)-deficiency under pathological conditions. Glia. 2013; 61:881–891. https://doi.org/10.1002/glia.22481. [PubMed: 23468421]

Bourquin AF, Suveges M, Pertin M, Gilliard N, Sardy S, Davison AC, … Decosterd I. Assessment and analysis of mechanical allodynia-like behavior induced by spared nerve injury (SNI) in the mouse. Pain. 2006; 122:14e11–e14. https://doi.org/10.1016/j.pain.2005.10.036. [PubMed: 16542774]

Brawek B, Garaschuk O. Microglial calcium signaling in the adult, aged and diseased brain. Cell Calcium. 2013; 53:159–169. https://doi.org/10.1016/j.ceca.2012.12.003. [PubMed: 23395344]

Cero C, Vostrikov VV, Verardi R, Severini C, Gopinath T, Braun PD, … Bartolomucci A. The TLQP-21 peptide activates the G-protein-coupled receptor C3aR1 via a folding-upon-binding mechanism. Structure. 2014; 22:1744–1753. https://doi.org/10.1016/j.str.2014.10.001. [PubMed: 25456411]

Chaplan SR, Bach FW, Pogrel JW, Chung JM, Yaksh TL. Quantitative assessment of tactile allodynia in the rat paw. Journal of Neuroscience Methods. 1994; 53:55–63. https://doi.org/0165-0270(94)90144-9 [pii]. [PubMed: 7990513]

Chen YC, Pristera A, Ayub M, Swanwick RS, Karu K, Hamada Y, … Okuse K. Identification of a receptor for neuropeptide VGF and its role in neuropathic pain. Journal of Biological Chemistry. 2013; 288:34638–34646. https://doi.org/10.1074/jbc.M113.510917. [PubMed: 24106277]

Chinnery HR, Ruitenberg MJ, McMenamin PG. Novel characterization of monocyte-derived cell populations in the meninges and choroid plexus and their rates of replenishment in bone marrow chimeric mice. Journal of Neuropathology & Experimental Neurology. 2010; 69:896–909. https://doi.org/10.1097/NEN.0b013e3181edbc1a. [PubMed: 20720507]

Clark AK, Gruber-Schoffnegger D, Drdla-Schutting R, Gerhold KJ, Malcangio M, Sandkuhler J. Selective activation of microglia facilitates synaptic strength. Journal of Neuroscience. 2015; 35:4552–4570. https://doi.org/10.1523/JNEUROSCI.2061-14.2015. [PubMed: 25788673]

Davoust N, Jones J, Stahel PF, Ames RS, Barnum SR. Receptor for the C3a anaphylatoxin is expressed by neurons and glial cells. Glia. 1999; 26:201–211. [PubMed: 10340761]

Decosterd I, Woolf CJ. Spared nerve injury: An animal model of persistent peripheral neuropathic pain. Pain. 2000; 87:149–158. [PubMed: 10924808]

Doolen S, Blake CB, Smith BN, Taylor BK. Peripheral nerve injury increases glutamate-evoked calcium mobilization in adult spinal cord neurons. Molecular Pain. 2012; 8:56. https://doi.org/10.1186/1744-8069-8-56. [PubMed: 22839304]

Fairbanks CA. Spinal delivery of analgesics in experimental models of pain and analgesia. Advanced Drug & Delivery Reviews. 2003; 55:1007–1041.

Fairbanks CA, Peterson CD, Speltz RH, Riedl MS, Kitto KF, Dykstra JA, … Vulchanova L. The VGF-derived peptide TLQP-21 contributes to inflammatory and nerve injury-induced hypersensitivity. Pain. 2014; 155:1229–1237. https://doi.org/10.1016/j.pain.2014.03.012. [PubMed: 24657450]

Farber K, Kettenmann H. Functional role of calcium signals for microglial function. Glia. 2006; 54:656–665. https://doi.org/10.1002/glia.20412. [PubMed: 17006894]

Gattlen C, Clarke CB, Piller N, Kirschmann G, Pertin M, Decosterd I, … Suter MR. Spinal cord T-cell infiltration in the rat spared nerve injury model: A time course study. International Journal of Molecular Science. 2016; 17:352. https://doi.org/10.3390/ijms17030352.

Griffin RS, Costigan M, Brenner GJ, Ma CH, Scholz J, Moss A, … Woolf CJ. Complement induction in spinal cord microglia results in anaphylatoxin C5a-mediated pain hypersensitivity. Journal of Neuroscience. 2007; 27:8699–8708. https://doi.org/27/32/8699 [pii] 10.1523/JNEUROSCI.2018–07.2007. [PubMed: 17687047]

Gruber-Schoffnegger D, Drdla-Schutting R, Honigsperger C, Wunderbaldinger G, Gassner M, Sandkuhler J. Induction of thermal hyperalgesia and synaptic long-term potentiation in the spinal cord lamina I by TNF-alpha and IL-1beta is mediated by glial cells. Journal of Neuroscience. 2013; 33:6540–6551. https://doi.org/10.1523/JNEUROSCI.5087-12.2013. [PubMed: 23575851]

Hagino Y, Kariura Y, Manago Y, Amano T, Wang B, Sekiguchi M, … Noda M. Heterogeneity and potentiation of AMPA type of glutamate receptors in rat cultured microglia. Glia. 2004; 47:68–77. https://doi.org/10.1002/glia.20034. [PubMed: 15139014]

Hannedouche S, Beck V, Leighton-Davies J, Beibel M, Roma G, Oakeley EJ, … Bassilana F. Identification of the C3a receptor (C3AR1) as the target of the VGF-derived peptide TLQP-21 in rodent cells. Journal of Biological Chemistry. 2013; 288:27434–27443. https://doi.org/10.1074/jbc.M113.497214. [PubMed: 23940034]

Hirasawa T, Ohsawa K, Imai Y, Ondo Y, Akazawa C, Uchino S, Kohsaka S. Visualization of microglia in living tissues using Iba1-EGFP transgenic mice. Journal of Neuroscience Research. 2005; 81:357–362. https://doi.org/10.1002/jnr.20480. [PubMed: 15948177]

Hunsberger JG, Newton SS, Bennett AH, Duman CH, Russell DS, Salton SR, Duman RS. Antidepressant actions of the exercise-regulated gene VGF. Nature Medicine. 2007; 13:1476–1482. https://doi.org/10.1038/nm1669.

Hylden JL, Wilcox GL. Intrathecal substance P elicits a caudally-directed biting and scratching behavior in mice. Brain Research. 1981; 217:212–215. [PubMed: 6167328]

Ji RR, Xu ZZ, Gao YJ. Emerging targets in neuroinflammation-driven chronic pain. Nature Review & Drug Discovery. 2014; 13:533–548. https://doi.org/10.1038/nrd4334. [PubMed: 24948120]

La Croix-Fralish ML, Austin JS, Zheng FY, Levitin DJ, Mogil JS. Patterns of pain: Meta-analysis of microarray studies of pain. Pain. 2011; 152:1888–1898. https://doi.org/10.1016/j.pain.2011.04.014. [PubMed: 21561713]

Lian H, Litvinchuk A, Chiang AC, Aithmitti N, Jankowsky JL, Zheng H. Astrocyte–microglia cross talk through complement activation modulates amyloid pathology in mouse models of Alzheimer's disease. Journal of Neuroscience. 2016; 36:577–589. https://doi.org/10.1523/JNEUROSCI.2117-15.2016. [PubMed: 26758846]

Lian H, Yang L, Cole A, Sun L, Chiang AC, Fowler SW, … Zheng H. NFkappaB activated astroglial release of complement C3 compromises neuronal morphology and function associated with Alzheimer's disease. Neuron. 2015; 85:101–115. https://doi.org/10.1016/j.neuron.2014.11.018. [PubMed: 25533482]

Lin WJ, Jiang C, Sadahiro M, Bozdagi O, Vulchanova L, Alberini CM, Salton SR. VGF and its C-terminal peptide TLQP-62 regulate memory formation in hippocampus via a BDNF-TrkB-dependent mechanism. Journal of Neuroscience. 2015; 35:10343–10356. https://doi.org/10.1523/JNEUROSCI.0584-15.2015. [PubMed: 26180209]

Liu GJ, Kalous A, Werry EL, Bennett MR. Purine release from spinal cord microglia after elevation of calcium by glutamate. Molecular Pharmacology. 2006; 70:851–859. https://doi.org/10.1124/mol.105.021436. [PubMed: 16760362]

Liu L, Tornqvist E, Mattsson P, Eriksson NP, Persson JK, Morgan BP, … Svensson M. Complement and clusterin in the spinal cord dorsal horn and gracile nucleus following sciatic nerve injury in the adult rat. Neuroscience. 1995; 68:167–179. [PubMed: 7477922]

Liu N, Zhang D, Zhu M, Luo S, Liu T. Minocycline inhibits hyperpolarization-activated currents in rat substantia gelatinosa neurons. Neuropharmacology. 2015; 95:110–120. https://doi.org/10.1016/j.neuropharm.2015.03.001. [PubMed: 25777286]

Moller T, Bard F, Bhattacharya A, Biber K, Campbell B, Dale E, … Boddeke HW. Critical data-based re-evaluation of minocycline as a putative specific microglia inhibitor. Glia. 2016; 64:1788–1794. https://doi.org/10.1002/glia.23007. [PubMed: 27246804]

Moss A, Ingram R, Koch S, Theodorou A, Low L, Baccei M, … Fitzgerald M. Origins, actions and dynamic expression patterns of the neuropeptide VGF in rat peripheral and central sensory neurones following peripheral nerve injury. Molecular Pain. 2008; 4:62. https://doi.org/10.1186/1744-8069-4-62. [PubMed: 19077191]

Murugan M, Sivakumar V, Lu J, Ling EA, Kaur C. Expression of *N*-methyl d-aspartate receptor subunits in amoeboid microglia mediates production of nitric oxide via NF-kappa B signaling pathway and oligodendrocyte cell death in hypoxic postnatal rats. Glia. 2011; 59:521–539. https://doi.org/10.1002/glia.21121. [PubMed: 21319220]

Nimmerjahn A, Kirchhoff F, Helmchen F. Resting microglial cells are highly dynamic surveillants of brain parenchyma *in vivo*. Science. 2005; 308:1314–1318. https://doi.org/10.1126/science.1110647. [PubMed: 15831717]

Peng HZ, Ma LX, Lv MH, Hu T, Liu T. Minocycline enhances inhibitory transmission to substantia gelatinosa neurons of the rat spinal dorsal horn. Neuroscience. 2016; 319:183–193. https://doi.org/10.1016/j.neuroscience.2016.01.047. [PubMed: 26826332]

Polfliet MM, Zwijnenburg PJ, van Furth AM, van der Poll T, Dopp EA, Renardel de Lavalette C, … van den Berg TK. Meningeal and perivascular macrophages of the central nervous system play a protective role during bacterial meningitis. Journal of Immunology. 2001; 167:4644–4650.

Riedl MS, Braun PD, Kitto KF, Roiko SA, Anderson LB, Honda CN, … Vulchanova L. Proteomic analysis uncovers novel actions of the neurosecretory protein VGF in nociceptive processing. Journal of Neuroscience. 2009; 29:13377–13388. https://doi.org/10.1523/JNEUROSCI.1127-09.2009. [PubMed: 19846725]

Rizzi R, Bartolomucci A, Moles A, D'Amato F, Sacerdote P, Levi A, … Pavone F. The VGF-derived peptide TLQP-21: A new modulatory peptide for inflammatory pain. Neuroscience Letters. 2008; 441:129–133. https://doi.org/10.1016/j.neulet.2008.06.018. [PubMed: 18586396]

Skaper SD, Argentini C, Barbierato M. Culture of neonatal rodent microglia, astrocytes, and oligodendrocytes from cortex and spinal cord. Methods & Molecular Biology. 2012; 846:67–77. https://doi.org/10.1007/978-1-61779-536-7_7.

Taves S, Berta T, Chen G, Ji RR. Microglia and spinal cord synaptic plasticity in persistent pain. Neural Plasticity. 2013; 2013:753656. https://doi.org/10.1155/2013/753656. [PubMed: 24024042]

Thakker-Varia S, Krol JJ, Nettleton J, Bilimoria PM, Bangasser DA, Shors TJ, … Alder J. The neuropeptide VGF produces antidepressant-like behavioral effects and enhances proliferation in the hippocampus. Journal of Neurosciences. 2007; 27:12156–12167. https://doi.org/10.1523/JNEUROSCI.1898-07.2007.

Tsuda M, Inoue K. Neuron–microglia interaction by purinergic signaling in neuropathic pain following neurodegeneration. Neuropharmacology. 2016; 104:76–81. https://doi.org/10.1016/j.neuropharm.2015.08.042. [PubMed: 26327676]

Twining CM, Sloane EM, Schoeniger DK, Milligan ED, Martin D, Marsh H, … Watkins LR. Activation of the spinal cord complement cascade might contribute to mechanical allodynia

induced by three animal models of spinal sensitization. Journal of Pain. 2005; 6:174–183. https://doi.org/10.1016/j.jpain.2004.11.011. [PubMed: 15772911]

Ulmann L, Hirbec H, Rassendren F. P2X4 receptors mediate PGE2 release by tissue-resident macrophages and initiate inflammatory pain. EMBO Journal. 2010; 29:2290–2300. https://doi.org/10.1038/emboj.2010.126. [PubMed: 20562826]

Urabe N, Naito I, Saito K, Yonezawa T, Sado Y, Yoshioka H, … Ninomiya Y. Basement membrane type IV collagen molecules in the choroid plexus, pia mater and capillaries in the mouse brain. Archives of Histology & Cytology. 2002; 65:133–143. [PubMed: 12164337]

Vasek MJ, Garber C, Dorsey D, Durrant DM, Bollman B, Soung A, … Klein RS. A complement–microglial axis drives synapse loss during virus-induced memory impairment. Nature. 2016; 534:538–543. https://doi.org/10.1038/nature18283. [PubMed: 27337340]

Wang X, Kim SU, van Breemen C, McLarnon JG. Activation of purinergic P2X receptors inhibits P2Y-mediated Ca^{2+} influx in human microglia. Cell Calcium. 2000; 27:205–212. [PubMed: 10858666]

Waschbisch A, Schroder S, Schraudner D, Sammet L, Weksler B, Melms A, … Linker RA. Pivotal role for CD16+ monocytes in immune surveillance of the central nervous system. Journal of Immunology. 2016; 196:1558–1567. https://doi.org/10.4049/jimmunol.1501960.

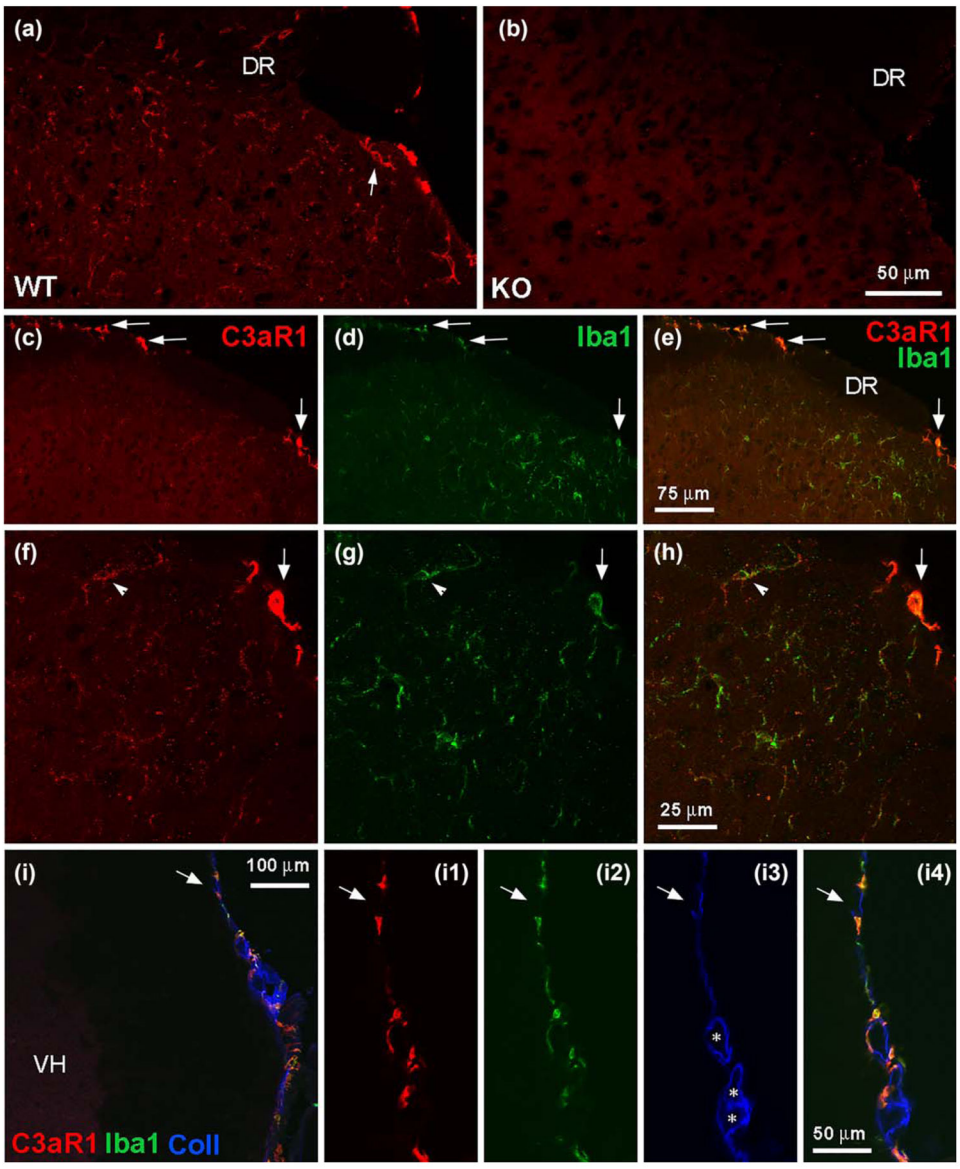

FIGURE 1.

Spinal localization of C3aR1. (a, b) C3aR1 immunolabeling in superficial dorsal horn from wild-type (WT) and knock-out (KO) mice (DR indicates dorsal roots). The arrow in A indicates a cellular profile that is outlined by C3aR1 immunoreactivity (–ir). Scale bar: 50 μm. (c–h) Immuno-histochemical analysis of C3aR1-ir (red) and its relationship to Iba1-ir (green) in dorsal horn. The dorsolateral region of the spinal cord in c–e is shown at higher magnification in f–h; e and h represent digital merging of c, d and f, g, respectively to show colocalization of labeling. C3aR1 and Iba1-ir overlap in fine processes and cellular profiles in superficial dorsal horn (f–h, arrowheads indicate the same cellular profile). Arrows in c–h indicate C3aR1/Iba1-positive profiles at the spinal cord perimeter. The image shown in f–h represents a projection of 3 optical sections, 1 μm apart. Scale bars: c–e, 75 μm; f–h, 25 μm. (i) C3aR1/Iba1-positive profiles at the spinal cord perimeter are associated with collagen IV (Coll) labeling that delineates the pia mater and subarachnoid blood vessels (VH indicates

ventral horn; * indicate subarachnoid blood vessels). The spinal cord perimeter is shown at higher magnification in (I1–4). The arrows indicate the same region in I and I1–4. Scale bars: I, 100 μm; I1–4, 50 μm

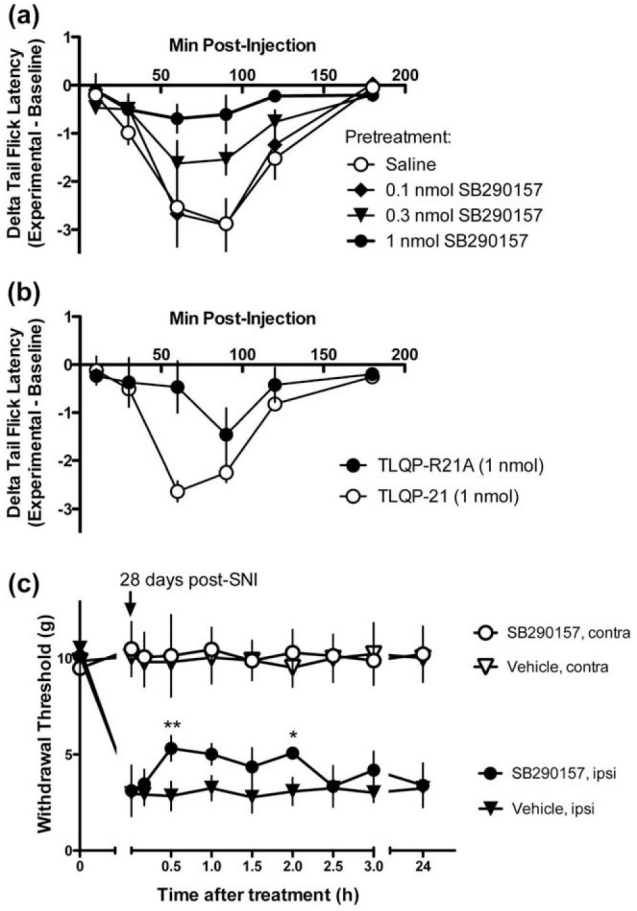

FIGURE 2.

C3aR1 mediates TLQP-21-evoked thermal hyperalgesia and contributes to nerve injury-induced hypersensitivity. (a) Thermal hyperalgesia induced by 1 nmol TLQP-21 (i.t.) is dose-dependently inhibited by pretreatment with the C3aR1 antagonist SB290157 (0.1–1 nmol, i.t.), $n = 6$ per treatment. (b) A modified TLQP-21 (R21A) that is unable to activate C3aR1 produces less hyperalgesia than TLQP-21 ($n = 4$ per treatment) ***$p < .001$ at 60 min, two-way repeated ANOVA, followed by Bonferroni *post hoc* test. (c) The reduction in mechanical withdrawal thresholds after SNI is partially reversed by SB290157. **$p < .01$ at 30 min, *$p < .05$ at 2 h after drug treatment, two-way repeated ANOVA, followed by Bonferroni *post hoc* test. (a–c) Data represent mean ± SEM

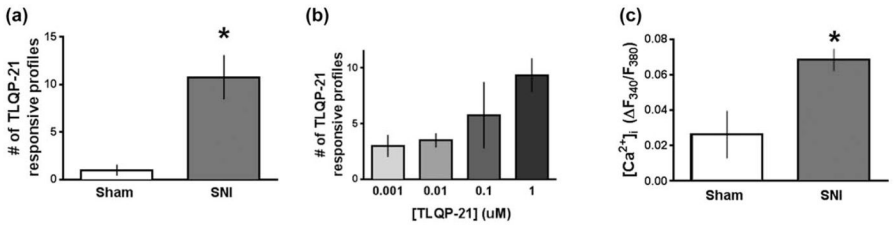

FIGURE 3.

TLQP-21 elicits spinal Ca^{2+}signaling that increases with neuropathic injury. (a) Live-cell Fura-2 ratiometric analysis in adult spinal cord slices 14 days after surgery reveals that SNI but not sham increases the total number of profiles within lamina II that are responsive to TLQP-21 (1 μM). (b) The number of profiles that are responsive to TLQP-21 (0.001–1 μM) increases in a concentration-dependent manner with an EC_{50} of 140.8 nM (n = 4 mice/group). (c) SNI increases peak amplitude of TLQP-21-evoked Ca^{2+} signals (n = 3–4/group). *p < .05, **p < .01 by t test. Data represent mean ± SEM

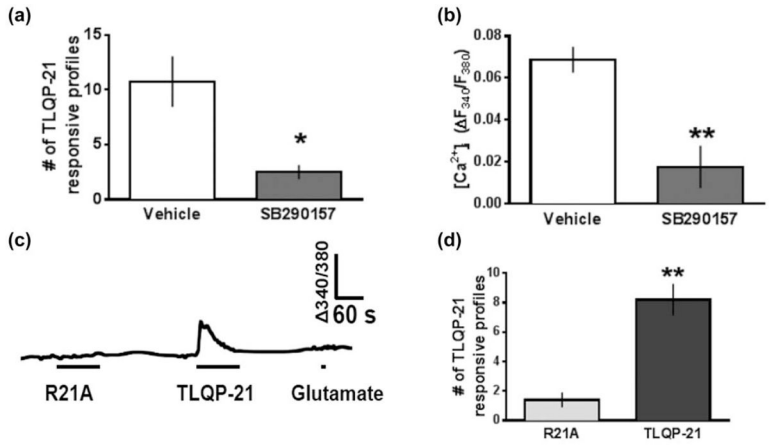

FIGURE 4.

TLQP-21-evoked Ca^{2+} transients in dorsal horn are C3aR1-dependent. (a) The total number of profiles responsive to 1 μM TLQP-21 and (b) peak TLQP-21-evoked Ca^{2+} signals decrease in the presence of 1 μM SB290157 (n = 4 mice/group). (c) Representative ratiometric traces of $[Ca^{2+}]_i$ in lamina II dorsal horn from a mouse spinal cord slice exposed to 1 μM R21A (90 s), 1 μM TLQP-21 (90 s) and 1 mM glutamate (10 s). Note that the TLQP-21 responsive profile does not respond to glutamate. (d) Total number of profiles that elicit a Ca^{2+} response to 1 μM R21A is significantly less than 1 μM TLQP-21 (n = 5 mice/group)

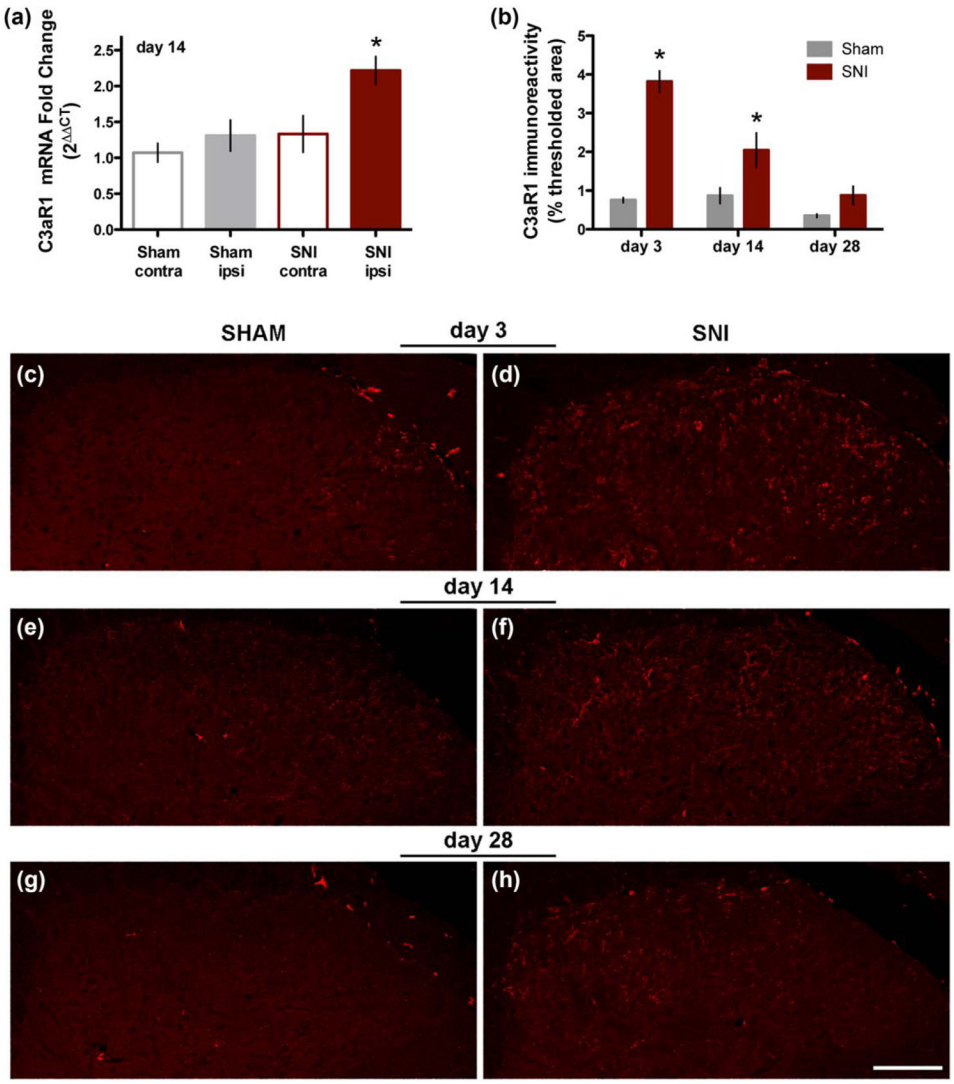

FIGURE 5.

Spinal expression of C3aR1 increases after nerve injury. (a) Real-time qPCR analysis demonstrates an increase in expression of C3aR1 mRNA in the ipsilateral spinal cord 14 days after SNI (n = 10–13 mice/group. *$p < .05$, one-way ANOVA followed by Tukey's *post hoc* test; data represent mean ± SEM). (b) Quantitative analysis of C3aR1 immunolabeling indicates that maximum increase in C3aR1 expression occurs 3 days post-SNI ($p < .1$ at day 3, $p < .05$ at day 14, $p = .06$ at day 28; t test). (c–h) Representative images illustrate the increase in C3aR1-ir at days 3 (C, sham; D, SNI), 14 (E, sham; F, SNI), and 28 (G, sham; H, SNI) after nerve injury. Scale bar: 100 μm

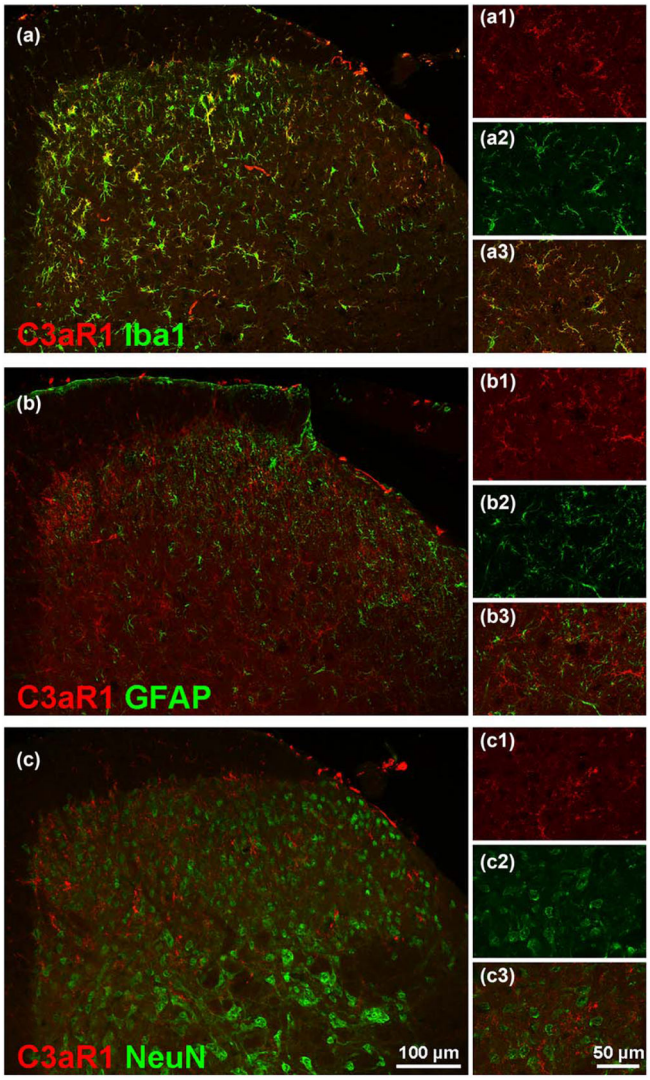

FIGURE 6.

Spinal C3aR1-ir is localized in microglia after nerve injury. Double-labeling for C3aR1 (red) and Iba1 (green, a), GFAP (green, b), and NeuN (green, c) in ipsilateral lumbar dorsal horn of SNI mice 14 days postsurgery. C3aR1-ir in dorsal horn colocalizes with Iba1-ir but not GFAP or NeuN-ir. Scale bar: 100 μm for a–c, 50 μm for a1–3, b1–3, c1–3

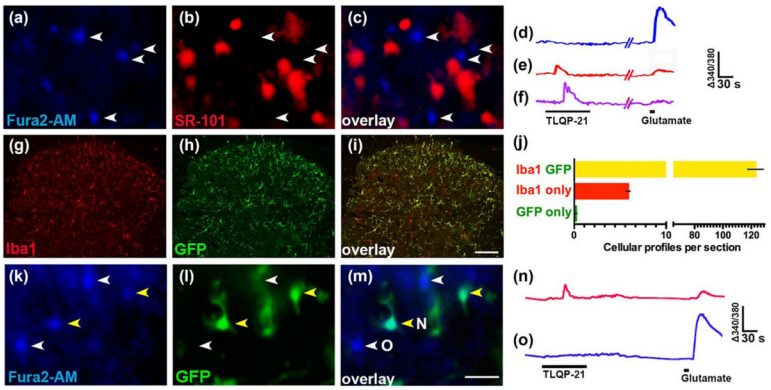

FIGURE 7.

TLQP-21 elicits Ca^{2+} signaling in spinal microglia. (a–c) Representative micrographs of dorsal horn simultaneously loaded with (a) Fura-2, (b) SR-101 (c) Merged image reveals the lack of overlap between Fura-2 and SR-101. (d–f) Representative ratiometric (Δ340/380 nm) traces of $[Ca^{2+}]_i$ signals from profiles that were responsive to (d) glutamate only, (e) both TLQP-21 and glutamate and (f) TLQP-21 only. (g–j) Double immunolabeling for Iba1 and GFP in spinal cord from Iba1-eGFP mice. Representative micrographs of dorsal horn show labeling for Iba1 (g) and GFP (h) and their overlap (i). Quantitative analysis of the colocalization (j). (k–m) Representative micrographs from an Iba1-eGFP mouse spinal cord slice loaded with Fura2-AM show overlap between GFP-positive cells and Fura-2. (n, o) Representative traces of $[Ca^{2+}]_i$ signals from Iba1-eGFP mice show the predominant responses seen in (n) GFP-positive profiles (yellow arrowheads in k and l) and (o) GFP-negative profiles (white arrowheads in K and L). Scale bars: a–c, k–m = 20 μm; g–i = 100 μm

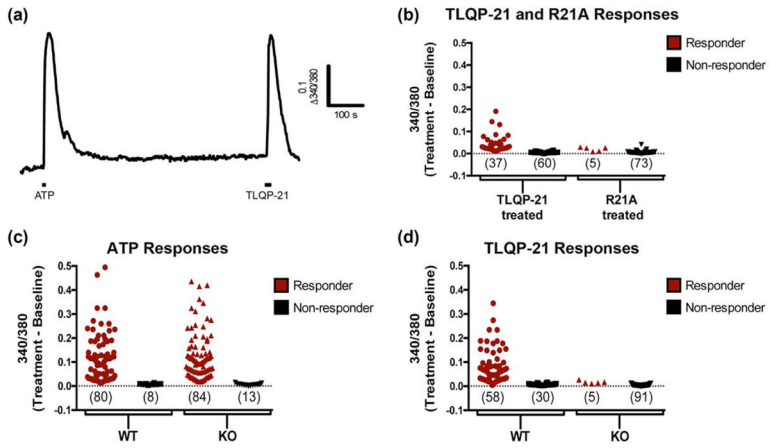

FIGURE 8.

TLQP-21 activates C3aR1 in cultured primary microglia. (a) Representative ratiometric (Δ340/380 nm) traces of ATP (100 μM) and TLQP-21 (10 μM)-evoked Ca^{2+} transients in microglial cells isolated from P1–3 neonatal brain from wild-type (WT) mice. (b) Scatter plot of peak response amplitudes to TLQP-21 and R21A in wild-type cultures demonstrates that the proportions of TLQP-21 and R21A responders and nonresponders are significantly different ($p < .0001$, Fisher's exact test). (c) Scatter plot of peak response amplitudes to ATP in cultures from WT and C3aR1 KO mice shows that the proportions of ATP responders and nonresponders in WT and KO cultures are not significantly different. (d) Scatter plot of peak response amplitudes to TLQP-21 in cultures from C3aR1 KO and WT mice shows that the proportions of TLQP-21 responders and nonresponders in WT and KO cultures are significantly different ($p < .0001$, Fisher's exact test). Each symbol in b–d represents a cell [Color figure can be viewed at wileyonlinelibrary.com]

TABLE 1

Ca^{2+} responses to glutamate in TLQP-21 responsive and nonresponsive cells

	None	Low	High	Total
TLQP-21 responder	35/76 (46%)	35/76 (46%)	6/76 (8%)	76/161
TLQP-21 nonresponder	N/A	34/85 (40%)	51/85 (60%)	85/161

Spinal cord slices were superfused with TLQP-21 (1 μM, 90 s), and then with glutamate (1 mM, 10 s). Profiles were classified as TLQP-21 'responders' if they exhibited increases in Ca^{2+} greater than 3% of baseline (noise accounts for roughly 3% change in baseline). Both responders and nonresponders were further categorized based on whether they exhibited no (<3% baseline), low (3–10% baseline), or high (>10% baseline) Ca^{2+} signals in response to glutamate.

TABLE 2

Ca^{2+} responses to glutamate in TLQP-21 responsive and nonresponsive cells: Iba1-eGFP positive and negative mice

eGFP(+) cells: 23/114 (20%)	**None**	**Low**	**High**	**Total**
TLQP-21 responder	3/22 (14%)	17/22 (77%)	2/22 (9%)	22/23
TLQP-21 nonresponder	1/1 (100%)	0/1 (0%)	0/1 (0%)	1/23
eGFP (−) cells: 91/114 (80%)	**None**	**Low**	**High**	**Total**
TLQP-21 responder	1/6(17%)	4/6 (67%)	1/6 (17%)	6/91
TLQP-21 nonresponder	0/85 (0%)	32/85 (38%)	53/85 (62%)	85/91

Spinal cord slices from mice expressing eGFP under the control of the Iba1 promoter were superfused with TLQP-21 (1 μM, 90 s), and then with glutamate (1 mM, 10 s). Of 114 cells tested, 23 (20%) were eGFP positive while 91 (80%) were eGFP negative. Within these two populations, profiles were classified as TLQP-21 ‘responders’ if they exhibited increases in Ca^{2+} greater than 3% of baseline (noise accounts for roughly 3% change in baseline). Both responders and nonresponders were further categorized based on whether they exhibited no (<3% baseline), low (3–10% baseline) or high (>10% baseline) Ca^{2+} signals in response to glutamate.